

An Isolation Transformer-less Single DC Source Fed Dual 5-leg Inverter Controlled 5-phase Induction Motor with Modified Direct Torque

Venkata Subba Reddy C. , and Swati Devabhaktuni , *Member, IEEE*

Abstract—A modified hysteresis torque controller is introduced into the direct torque control scheme of a 5-phase open-end winding induction motor, aimed at enhancing steady-state performance by minimizing torque, flux ripple, and current total harmonic distortion (%THD) with the dual 5-leg inverter configuration. The proposed Direct Torque Control (DTC) strategy utilizes a common DC source for both converters without the need for a bulky isolation transformer, accomplished by nullifying common mode voltage in the dual inverter open-end winding configuration. This proposed technique employs 30 virtual voltage vectors (VVs) generated from the dual inverter configuration, strategically categorized as small, large, and medium voltage vectors. These 30 VVs are instrumental in forming a 7-level torque controller and a 3-level torque controller in the proposed DTC scheme. In contrast to the existing DTC method, which uses 20 virtual voltage vectors from a dual 5-leg inverter configuration and grapples with challenges like high current harmonic distortion, torque ripple, and flux ripple, the proposed control scheme introduces a new 7-level torque hysteresis controller. The outcome is reduced torque and flux ripple, along with minimized harmonic content across various speeds and loading conditions without disturbing the dynamics. Experimental hardware results are scrutinized, comparing the classical DTC with the proposed DTC schemes in open-end winding induction motors, aiming to know the superior qualities of the proposed control approach.

Link to graphical and video abstracts, and to code: <https://latamf.ieeer9.org/index.php/transactions/article/view/8474>

Index Terms—Direct Torque Control, dual 5-leg inverter, flux ripple, torque ripple, current %THD, 5-phase open-end winding induction motor

I. INTRODUCTION

Due to the advancement of fast-operating power semiconductor switches and fast DSP processors, multi-phase induction motors have gained more interest among researchers and industry experts over the last two decades [1], [2]. Among multi-phase motors, 5-phase machines show benefits over conventional 3-phase machines such as high torque per unit volume [3], less torque ripple, great fault tolerant [4], [5], less magnitude and high-frequency torque ripple [6], reduced per phase power which makes 5-phase motor drive adaptable for electric transportation [7]. Several advanced control schemes available for control of 3-phase machines such as field-oriented control schemes, and predictive control schemes are adopted to control multi-phase electrical machines to make electric drive smoother and faster

[8], [9]. Conversely, these advanced control methods suffer from complicated design, cost function adjustment, and high computational burden [8], [10]. Direct torque control (DTC) is an alternative control scheme and attains good attention in the process industries due to its simplicity and excellent dynamics even though it suffers from variable switching frequency, high flux, and torque ripples [11]. The influence of applied voltage vectors on torque and flux is discussed in the classical DTC technique [12], [13].

The advanced control schemes cannot be applied directly to multi-phase motors as they contain non-torque-producing plane components and torque-producing components, creating unnecessary power losses and phase current distortion [10]. Hence, it is necessary to eliminate/minimize harmonic (xy) plane components while implementing any control scheme in multi-phase machines. In literature, numerous works have been done to mitigate the shortcomings of the conventional DTC method in 5-phase induction motors (FPIM). Several novel DTC schemes are implemented to control the five-phase induction in literature [14]-[19]. They are mainly focused on xy plane components elimination or reduction, torque/flux ripple reduction, constant switching frequencies, and common mode voltage mitigation. Initially, a classical DTC is implemented in an FPIM with a 2-level 5-leg inverter [14] which suffers from the drawbacks of classical DTC [11] and xy plane components are partially eliminated. In [15], basic 3-level DTC extended with the complete elimination of xy plane components with the idea of virtual voltage vectors. In [16], low-speed performance improved with a five-level torque controller and selection of nearest vectors under low speed which won't make zero harmonic plane components. In [17], Payami et.al tried to improve the flux pattern under dynamics at low speed by replacing the null vectors with small vectors in the lookup table. A duty-based constant switching frequency torque (CST) controller is proposed in a 5-phase induction motor [18] to maintain constant switching frequency and to reduce the torque ripple and it is not focused on xy plane components elimination. In [19] and [20], two space vector-based DTC schemes are developed to get constant switching frequency and eliminate xy plane components and they need more PI controllers. In [21], a 5-level CST controller is developed with large and medium voltage vectors in a 5-phase induction motor and it won't eliminate xy plane components elimination.

Recent research focuses on using multi-level inverters (MLI) for high/medium power industrial motors. These inverters offer advantages like fault tolerance, redundant switching states, modularity, and reduced torque and flux

Venkata S. Reddy C. and Swati Devabhaktuni are with the National Institute of Technology, Warangal, Telangana-506004, India (e-mails: cvsreddy@student.nitw.ac.in and swatikjm@nitw.ac.in).

ripple. Several research works have been done in the literature on different MLI-fed 3-phase drives [22]-[24]. In [22], a modified DTC is implemented on a neutral point inverter-controlled 3-phase drive and addresses the DC link voltage fluctuations. In [23], a DTC is implemented on a cascaded H-bridge-based MLI-fed 3-phase induction motor to improve the voltage profile which requires independent DC sources. In [24], DTC is implemented on a flying capacitor-based MLI-fed 3-phase induction motor which suffers from voltage balancing issues, and variable capacitor stresses. The researchers started to focus on MLI-fed 5-phase induction motors to combine the advantages associated with the MLI and multi-phase drives. In [25], a DTC with five-level and seven-level torque controllers for a 3-level neutral point clamped-converter fed 5-phase induction motor is executed which suffers drawbacks associated with the converter such as capacitor imbalance and neutral point shifting. In [26], a modified DTC with a novel neutral point balancing scheme is implemented in a 3-level neutral point inverter-fed 5-phase induction motor.

Apart from above mentioned various multi-level inverter topologies, dual inverter configuration attains good attention due to their special features like reduced DC-link voltage, no capacitor neutral balance issue, no need of clamping diodes, and no flying capacitors required, and simple configuration [27]. Recently several researchers focused on working on dual-inverter controlled 5-phase induction motors to adopt features associated with dual inverter configuration [28]-[34]. In [28] and [29], two different space voltage vector modulation schemes are implemented to eliminate common mode voltage/current in dual inverter-controlled open-end winding five-phase induction motor (FP-OEWIM). A 9-level torque controller-based DTC is implemented in [30] with the developed four sets of voltage vectors in a dual inverter-controlled FPOEWIM to reduce torque and flux ripple but the author does not consider harmonic plane components which creates unnecessary power loss and common mode voltage not taken into consideration. In [31], a basic 3-level hysteresis torque controller is employed in DTC of dual inverter-controlled FPOEWIM with 10 virtual voltage vectors (VVV) and it exhibits high flux torque ripple and current harmonic content. A new 5-level torque controller is introduced in DTC of dual inverter fed FPOEWIM with 20 VVV to reduce flux ripple torque ripple and current THD [32] and still, it exhibits high torque-flux ripple, and current distortion and does not eliminate harmonic plane components. In [33], the author extended the work done in [32] by eliminating harmonic plane components in a dual inverter-controlled 5-phase induction motor. The work presented in [34] introduces a 7-level Direct Torque Control (DTC) of a dual inverter-fed FPOEWIM that primarily focuses on simulation results with 30 virtual voltage vector combinations with limited explanation, and not discussed motor dynamics. The proposed research work builds upon [34] by incorporating valid experimental results under both steady-state and dynamics, conducting an in-depth analysis, and comparing with existing literature.

The proposed Direct Torque Control (DTC) scheme employs a 7-level hysteresis torque controller with all 30 VVV's for high speeds to reach faster torque response which is really needed under high speeds and fine torque variation. The proposed DTC also uses 3-level hysteresis torque

controllers with only small voltage vectors to further minimize both torque and flux ripple for low speeds. The proposed DTC control method minimizes the torque ripple, flux ripple, and current Total Harmonic Distortion (THD) along with the elimination of harmonic (xy) plane components and common mode voltage (CMV). The elimination of CMV in the dual inverter configuration increases the motor life span as this CMV is the main source of EMI and bearing currents. The zero CMV in dual inverter allows the use of a single common DC source without the isolation transformer, which will reduce the complexity, cost, size, and weight of the system [28].

The remaining article is organized as follows. Section II discusses the generation of switching voltage vectors in a dual inverter. Section III discusses the execution of the proposed DTC control method with a block diagram and switching tables. Section IV discusses the experimental data analysis. Finally, section V gives the conclusion of the proposed work.

II. GENERATION OF SWITCHING STATE VECTORS IN A DUAL 5-LEG INVERTER CONFIGURATION OF OEWIM

A. Virtual Voltage Vector Generation in a 5-leg Inverter

A 2-level 5-leg inverter shown in Fig. 1 produces 32 switching states and the switching states are classified as large vectors (0.6472V_{dc}), medium vectors (0.4V_{dc}), small vectors (0.2472V_{dc}), and null vectors (0V_{dc}) in the harmonic (xy) and fundamental (αβ) plane.

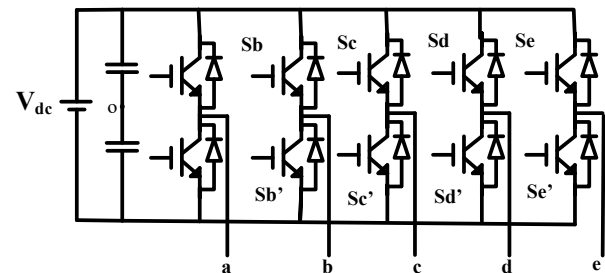


Fig. 1. 2-level 5-leg inverter circuit configuration.

The switching state vector location and magnitude in the αβ and xy plane are obtained from (1) and (2). These space vector locations are shown in Fig. 2.

$$V_{s(\alpha\beta)} = \frac{2}{5} V_{dc} (S_a + S_b e^{j\frac{2\pi}{5}} + S_c e^{j\frac{4\pi}{5}} + S_d e^{j\frac{-4\pi}{5}} + S_e e^{j\frac{-2\pi}{5}}) \quad (1)$$

$$V_{s(xy)} = \frac{2}{5} V_{dc} (S_a + S_b e^{j\frac{-4\pi}{5}} + S_c e^{j\frac{2\pi}{5}} + S_d e^{j\frac{-2\pi}{5}} + S_e e^{j\frac{4\pi}{5}}) \quad (2)$$

where

$V_{s(\alpha\beta)}$ =fundamental plane voltage vector

$V_{s(xy)}$ =harmonic plane voltage vector

V_{dc} =DC-bus voltage

S_a, S_b, S_c, S_d, S_e =switch status (1 or 0)

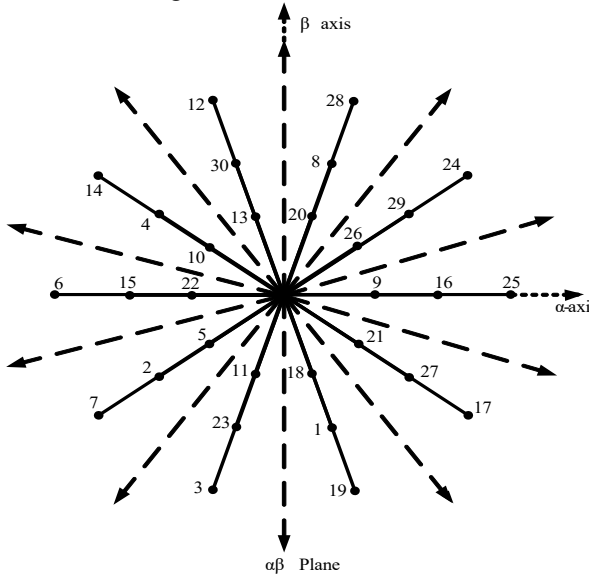
From Fig. 2, As can be noticed that the fundamental (αβ) plane large voltage vectors appear as harmonic (xy) plane small vectors with the opposite direction, and vice versa. similarly, the αβ plane medium voltage vectors appear as xy plane medium voltage vectors with the same direction [15]. The xy plane components cause ohmic losses for the

distributed winding machine, whereas the components of the fundamental plane produce useful torque. Hence, to avoid the significant power loss caused by xy plane currents, it is essential to eliminate the xy plane components. The elimination of xy plane components is done with the volt-second balance method as explained in [21]. Since the ratio of the magnitudes of the medium vector (e.g. 16) and the small vector (e.g. 25) is 1/0.6181 in the xy plane, the ratio of dwell times for the medium and small vector states is chosen as 0.6181 to produce a zero mean vector in the xy plane, as shown in Fig. 3(a), resulting in zero harmonic currents [17]. The resultant voltage V_1 in the $\alpha\beta$ plane (produced by switching states 25,16) will be computed as in (3) and illustrated in Fig. 3(a).

$$T_s V_1 = t_1 * 25 + t_2 * 16$$

$$V_1 = 0.553V_{dc} \angle 0^\circ \tag{3}$$

Where 16=Medium vector= $0.4V_{dc} \angle 0^\circ$
 25=Large vector= $0.642V_{dc} \angle 0^\circ$



t_1 =Dwell time of large vector= $0.618T_s$
 t_2 =Dwell time medium vector= $0.382T_s$
 T_s =Total sample time= t_1+t_2

From the medium vector 16 and small vector 9 of the inverter, the small virtual vectors are produced below (4)

$$T_s V_{11} = t_1 * 16 + t_2 * 9$$

$$V_{11} = 0.342V_{dc} \angle 0^\circ \tag{4}$$

Where 16=Medium vector= $0.4V_{dc} \angle 0^\circ$
 9=Small vector= $0.247V_{dc} \angle 0^\circ$
 t_1 =Dwell time of large vector= $0.618T_s$
 t_2 =Dwell time medium vector= $0.382T_s$
 T_s =Total sample time= t_1+t_2

As shown in Fig. 3(b), the selected inverter switching states with the computed dwell periods create 10 large virtual voltage vectors V_1 to V_{10} and 10 small virtual voltage vectors V_{11} to V_{20} with magnitudes of $0.553V_{dc}$ and $0.342V_{dc}$ respectively.

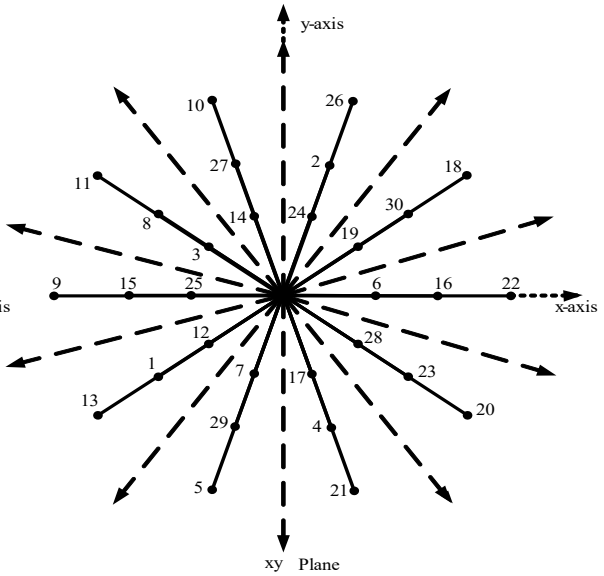
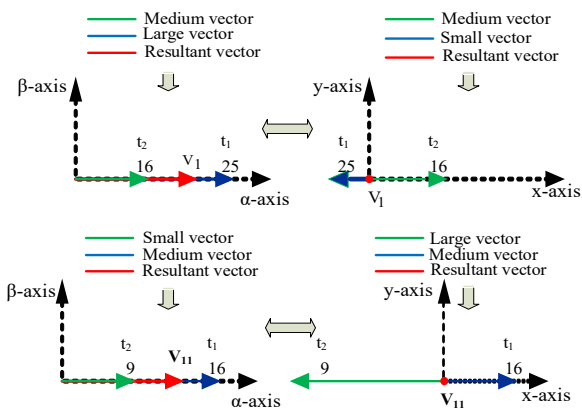
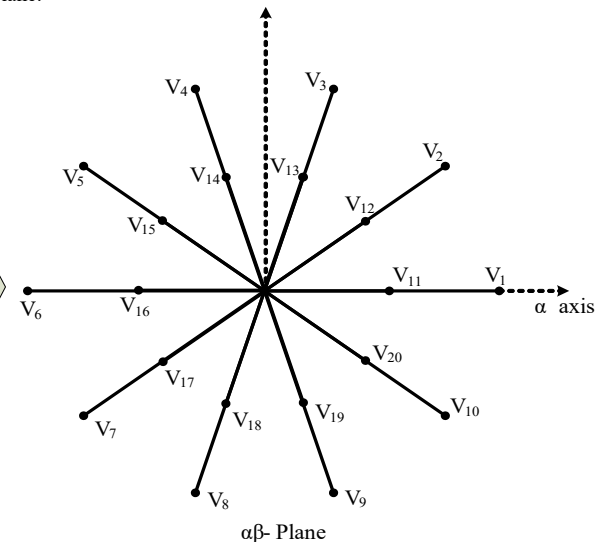


Fig. 2. Switching vectors space location of 5-phase inverter in $\alpha\beta$ plane and xy plane.



(a) Virtual Vector Generation



(b) Space Virtual Vector Diagram

Fig. 3. (a) Resultant virtual voltage vector V_1 and V_{11} generation in both $\alpha\beta$ - plane and xy-plane (b) Virtual voltage vector space diagram in $\alpha\beta$ - plane.

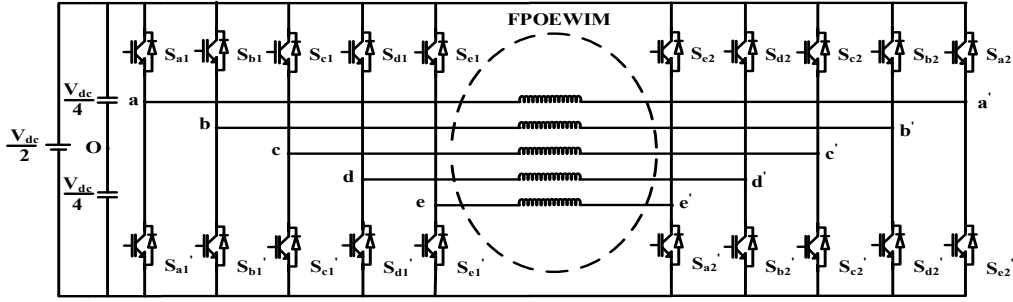


Fig. 4. Single DC source fed Dual inverter controlled open-end winding 5-phase induction motor.

B. Vectors Formation in Dual Inverter Fed FPOEWIM:

The power circuit of a dual inverter-fed FPOEWIM, illustrated in Fig. 4, incorporates two 5-leg inverters, an open-end winding induction motor, and a single DC source. The common mode voltage (CMV) of each single 2-level 5-leg inverter can be expressed with inverter pole voltages as in (5) [30].

$$\begin{aligned} V_{cmvI} &= \left(\frac{1}{5}\right) * (V_a + V_b + V_c + V_d + V_e) \\ V_{cmvII} &= \left(\frac{1}{5}\right) * (V_{a'} + V_{b'} + V_{c'} + V_{d'} + V_{e'}) \end{aligned} \quad (5)$$

Where,

V_a, V_b, V_c, V_d, V_e =Inverter I pole voltages ($V_x=S_x*V_{dc}/2$)
 $V_{a'}, V_{b'}, V_{c'}, V_{d'}, V_{e'}$ = Inverter II pole voltages($V_x=S_x*V_{dc}/2$)
 S_x and $S_{x'}$ =0 or 1; x =phase a..e.; x' =phase a'..e'.

The CMV for the dual 5-leg inverter (DI) configuration can be expressed as (6)

$$V_{cmvDI} = V_{cmvI} - V_{cmvII} \quad (6)$$

The virtual voltage vectors of inverter I and Inverter II are used to create the resultant voltage vectors of the dual 5-leg inverter, such that each inverter should generate equal common mode voltages i.e $V_{cmvI}=V_{cmvII}$.

$$V_{cmvDI} = V_{cmvI} - V_{cmvII} = 0 \quad (7)$$

When choosing the switching vectors of inverter I and inverter II to create the resultant vector of a dual inverter, the phase difference of $n*2/5$ ($n=1..5$) between the switching states of inverter I and inverter II is maintained, and as a result, inverter I and inverter II produce equal CMV, leads to zero common mode voltage for dual 5-leg inverter.

The available twenty active VVV's of each inverter will form 30 voltage vectors in the dual inverter configuration shown in Fig. 5 with zero CMV and these 30 voltage vectors grouped into medium (V_M), large (V_L), and small (V_S) vectors as shown in Fig. 5. The voltage vector V_{M1} formed from inverter I vector V_1 and inverter II vector V_9 as shown in (8). Similarly, 30 virtual voltage vectors are formed from adjacent and non-adjacent voltage vectors of inverter I and II as in (8), (9), and (10). These 30 voltage vectors form a 7-level and a 3-level torque controller for the proposed DTC scheme.

Formation of adjacent line voltages:

$$\begin{aligned} V_{M1} &= V_1 - V_9 \\ V_{M1} &= 0.553V_{dc}\angle 0 - 0.553V_{dc}\angle\left(\frac{9\pi}{5}\right) = 0.623V_{dc}\angle\left(\frac{3\pi}{10}\right) \quad (8) \\ V_{S1} &= V_{11} - V_{19} \end{aligned}$$

$$V_{S1} = 0.342V_{dc}\angle 0 - 0.342V_{dc}\angle\left(\frac{9\pi}{5}\right) = 0.385V_{dc}\angle\left(\frac{3\pi}{10}\right) \quad (9)$$

Formation of non-adjacent line voltages:

$$\begin{aligned} V_{L1} &= V_1 - V_7 \\ V_{L1} &= 0.553V_{dc}\angle 0 - 0.553V_{dc}\angle\left(\frac{6\pi}{5}\right) = 1.05V_{dc}\angle\left(\frac{\pi}{10}\right) \quad (10) \end{aligned}$$

The classic DTC [31] in dual inverter-fed FPOEWIM uses a 3-level torque hysteresis controller with large (V_L) vectors only, which yields high torque ripple and flux ripples and current harmonic distortion. A 5-level DTC is introduced with 20 VVV's (both large V_L , and medium V_M) for a five-phase dual inverter configuration [33] and still, it exhibits high harmonic current distortion and torque ripple. The proposed works in [31] and [33] also under-utilizes the switching states combinations of DI. The 7-level torque hysteresis controller is introduced to complete utilization 30 voltage vectors in the proposed DTC method's lookup table I during high speeds (speed > 300 rpm), which assists in reduced torque and flux ripple. Small voltage vectors are applied at low speeds (speed \leq 300 rpm) with a separate 3-level torque hysteresis controller and 3-level lookup table II, which results in further decreased torque ripple and flux ripple. The 3-level DTC [31], 5-level DTC [33], and proposed DTC scheme are compared with the same torque hysteresis controller band of 0.3 Nm (10% of rated torque) and same flux hysteresis controller band of 0.005Wb (4% of rated flux) with sample time 100e-6 sec.

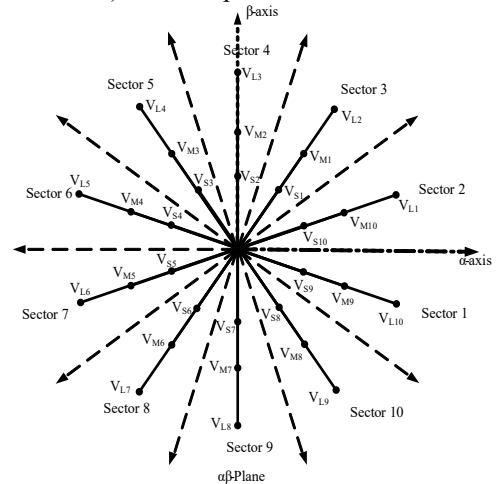


Fig. 5. Space vector diagram of virtual voltage vectors of dual inverter.

III. OPERATION OF PROPOSED DIRECT TORQUE CONTROL METHOD OF DUAL 5-LEG INVERTER CONTROLLED FPOEWIM

The block diagram illustration of the proposed DTC method of dual inverter-controlled FPOEWIM is shown in Fig. 6 and it contains a speed PI controller, speed encoder,

torque-flux estimation block, 7-level/3-level torque hysteresis controller, 2-level flux hysteresis controller, 2-level 5-leg inverters, and five-phase open-end winding induction motor. The suitable voltage vector is selected based on the obtained torque error, flux error, and sector information from the lookup table to meet the required torque and flux demands. The speed error is processed through the PI controller, creating a reference torque (T_e^*). This reference torque (T_e^*) and a reference flux (Ψ_s^*) are compared with the actual torque and actual flux, showing the differences as torque error (T_{err}) and flux error (Ψ_{serr}). The suitable voltage vector is selected based on the torque and flux error, and sector information from a lookup table. The desired changes in torque and flux can be obtained by applying suitable voltage vectors in a sample period T_s and it influences the flux directly as in (11) and the torque is mainly influenced by a change in stator flux angle with respect to rotor flux vector ($\Delta\theta$) as in (12) [18].

$$\Delta\Psi_s = (V_s - R_s i_s) \Delta T_s \quad (11)$$

$$\Delta T_e = \frac{5P}{2} \frac{L_m}{L_r L_{ss}} (|\Psi_s + \Delta\Psi_s|) (|\Psi_r|) \sin(\Delta\theta) \quad (12)$$

The stator flux and torque are estimated as below [18].

The stator voltage balancing equation is written as (13)

$$V_s = I_s R_s + \frac{d\Psi_s}{dt} \quad (13)$$

Where V_s = stator phase voltage in volts
 I_s = stator phase current in amperes
 R_s = stator resistance in ohms

The stator flux (Ψ_s) estimated from (14) as below

$$\Psi_s = \int (V_s - I_s R_s) dt \quad (14)$$

The electromagnetic torque (T_e) is estimated as below (15)

$$T_e = \frac{5P}{2} \text{imag}(\Psi_s^* I_s) \quad (15)$$

Where P- Induction motor stator poles

In the proposed DTC control method of DI-FPOEWIM, 30 virtual voltage vectors ($V_{L1} \dots V_{L10}$; $V_{M1} \dots V_{M10}$; $V_{S1} \dots V_{S10}$) and two null voltage vectors (V_0, V_{31}) are used to control the speed of the induction motor. The 7-level torque controller's upper band and lower band are divided into three parts according to the vector magnitude ratio below (16)

$$T_{stat} = +3 \text{ for } T_{err} > +0.3$$

$$T_{stat} = +2 \text{ for } T_{err} < +0.3 \text{ \& } T_{err} > +0.18$$

$$T_{stat} = +1 \text{ for } T_{err} < +0.18 \text{ \& } T_{err} > +0.11$$

$$T_{stat} = 0 \text{ for } T_{err} < +0.11 \text{ \& } T_{err} > -0.11$$

$$T_{stat} = -1 \text{ for } T_{err} < -0.11 \text{ \& } T_{err} > -0.18$$

$$T_{stat} = -2 \text{ for } T_{err} < -0.18 \text{ \& } T_{err} > -0.3$$

$$T_{stat} = -3 \text{ for } T_{err} < -0.3$$

(16)

Where T_{err} = torque error = $T_c^* - T_c$

T_{stat} = torque controller output status

Upper/lower hysteresis band = 0.3 Nm

The 2-level flux controller band is divided into the lower band and upper band as shown below (17)

$$\Psi_{stat} = +1 \text{ for } \Psi_{serr} > 0.005$$

$$\Psi_{stat} = -1 \text{ for } \Psi_{serr} < -0.005$$

(17)

Where Ψ_{serr} = flux error = $\Psi_s^* - \Psi_{sc}$

Ψ_{stat} = flux controller output status

Upper/lower hysteresis band = 0.005 Wb

With the information of torque controller status, flux controller status, and flux vector sector information; the suitable switching vectors are chosen as shown in lookup Table I and Table II.

TABLE I
SWITCHING VOLTAGE VECTOR SELECTION TABLE FOR HIGH SPEEDS

Ψ_{stat}	T_{stat}	Sector									
		1	2	3	4	5	6	7	8	9	10
1	3	V_{L2}	V_{L3}	V_{L4}	V_{L5}	V_{L6}	V_{L7}	V_{L8}	V_{L9}	V_{L10}	V_{L1}
1	2	V_{M1}	V_{M2}	V_{M3}	V_{M4}	V_{M5}	V_{M6}	V_{M7}	V_{M8}	V_{M9}	V_{M10}
1	1	V_{S1}	V_{S2}	V_{S3}	V_{S4}	V_{S5}	V_{S6}	V_{S7}	V_{S8}	V_{S9}	V_{S10}
1	0	Null									
1	-1	V_{S8}	V_{S9}	V_{S10}	V_{S1}	V_{S2}	V_{S3}	V_{S4}	V_{S5}	V_{S6}	V_{S7}
1	-2	V_{M8}	V_{M9}	V_{M10}	V_{M1}	V_{M2}	V_{M3}	V_{M4}	V_{M5}	V_{M6}	V_{M7}
1	-3	V_{L9}	V_{L10}	V_{L1}	V_{L2}	V_{L3}	V_{L4}	V_{L5}	V_{L6}	V_{L7}	V_{L8}
-1	3	V_{L4}	V_{L5}	V_{L6}	V_{L7}	V_{L8}	V_{L9}	V_{L10}	V_{L1}	V_{L2}	V_{L3}
-1	2	V_{M3}	V_{M4}	V_{M5}	V_{M6}	V_{M7}	V_{M8}	V_{M9}	V_{M10}	V_{M1}	V_{M2}
-1	1	V_{S3}	V_{S4}	V_{S5}	V_{S6}	V_{S7}	V_{S8}	V_{S9}	V_{S10}	V_{S1}	V_{S2}
-1	0	Null									
-1	-1	V_{S6}	V_{S7}	V_{S8}	V_{S9}	V_{S10}	V_{S1}	V_{S2}	V_{S3}	V_{S4}	V_{S5}
-1	-2	V_{M6}	V_{M7}	V_{M8}	V_{M9}	V_{M10}	V_{M1}	V_{M2}	V_{M3}	V_{M4}	V_{M5}
-1	-3	V_{L7}	V_{L8}	V_{L9}	V_{L10}	V_{L1}	V_{L2}	V_{L3}	V_{L4}	V_{L5}	V_{L6}

TABLE II
SWITCHING VOLTAGE VECTOR SELECTION TABLE FOR LOW SPEEDS

Ψ_{stat}	T_{stat}	Sector									
		1	2	3	4	5	6	7	8	9	10
1	1	V_{S1}	V_{S2}	V_{S3}	V_{S4}	V_{S5}	V_{S6}	V_{S7}	V_{S8}	V_{S9}	V_{S10}
1	0	Null									
1	-1	V_{S8}	V_{S9}	V_{S10}	V_{S1}	V_{S2}	V_{S3}	V_{S4}	V_{S5}	V_{S6}	V_{S7}
-1	1	V_{S3}	V_{S4}	V_{S5}	V_{S6}	V_{S7}	V_{S8}	V_{S9}	V_{S10}	V_{S1}	V_{S2}
-1	0	Null									
-1	-1	V_{S6}	V_{S7}	V_{S8}	V_{S9}	V_{S10}	V_{S1}	V_{S2}	V_{S3}	V_{S4}	V_{S5}

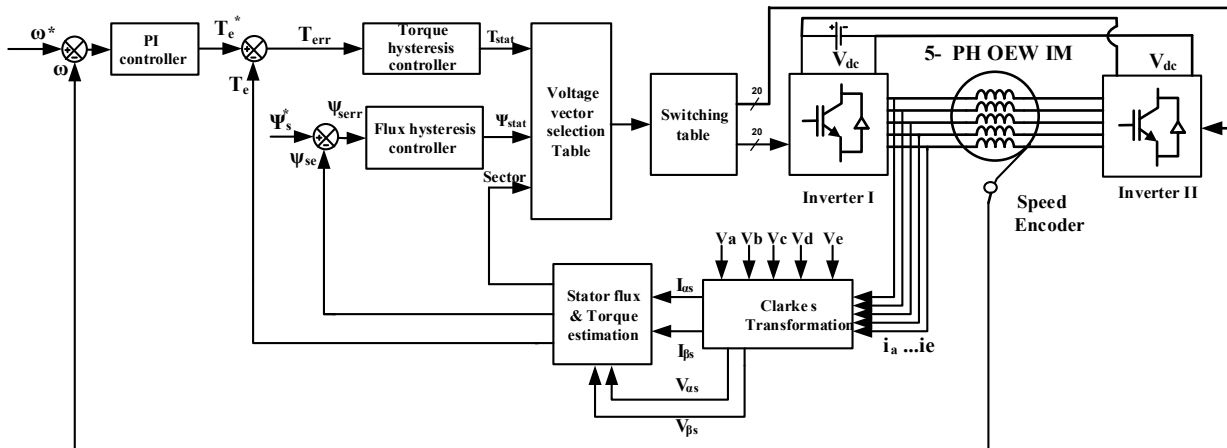


Fig. 6. Block diagram representation of the proposed DTC of dual inverter-controlled five-phase Induction Motor.

IV. HARDWARE RESULTS AND DISCUSSION

The proposed Direct Torque Control (DTC) scheme for driving a dual five-leg inverter-fed Five-Phase Open-End Winding Induction Motor (FPOEWIM) is systematically compared with existing works [31], [33] through valid experimental findings. The hardware experimental prototype, depicted in Fig. 7, comprises a 1-phase autotransformer, a 1 HP five-phase OEWIM coupled with a 1 HP DC generator load, LV 25-P voltage sensors, a resistive light load bank, and LEM LA 25-P current sensors. Additionally, it incorporates two IGBT five-leg inverter power modules. Both existing DTC control methods [31], [33] and the proposed DTC control method are executed with the same torque hysteresis band (HB_{T_c}) of 10% rated torque and flux hysteresis band (HB_{ψ_c}) of 4% rated flux. The subsequent sections investigate the examination of results obtained from the 3-level DTC [31], 5-level DTC [33], and the proposed DTC methods to assess the effectiveness of the proposed DTC control scheme.

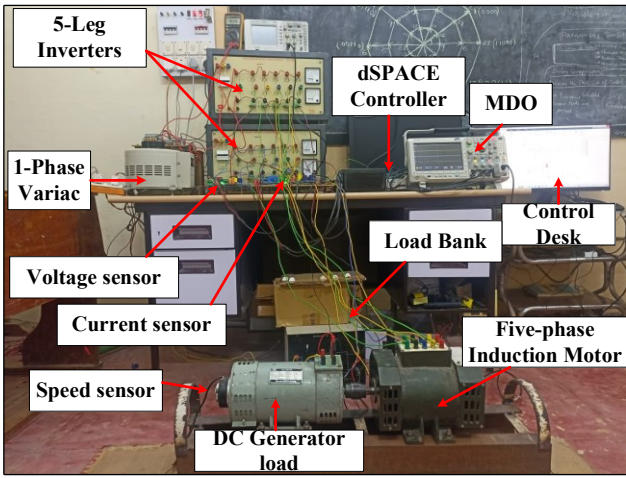


Fig. 7. Experimental Setup of dual 2-level 5-leg inverter fed open-end winding five-phase induction motor.

A. Steady-state Response Analysis

The steady-state performance evaluation of the FPOEWIM is examined in terms of flux ripple, torque ripple, and current harmonic distortion across different speeds and loading conditions for three control methods: 3-level DTC [31], 5-level DTC [33], and the proposed DTC control methods. This comprehensive analysis aims to assess the superiority of the modified lookup table-based proposed DTC method. The computation of torque and flux ripples employs equation (18), utilizing real-time data points from the steady-state hardware results for all three control schemes [18]. This rigorous assessment provides a detailed understanding of the performance characteristics and highlights the effectiveness of the proposed DTC approach.

$$\text{torque/flux}_{\text{ripple}} = \sqrt{\frac{1}{K} \sum_{x=1}^K (Y(i) - Y_{\text{avg}})^2} \quad (18)$$

Where Y_{avg} =average torque/flux over K samples

$Y(x)$ =torque/flux value at the x^{th} instant

1) Torque and Flux Ripple Analysis

a) No Load Condition: In Fig. 8, the torque and flux patterns under no load are illustrated at speeds (I) 1400rpm and (II) 100rpm. Notably, I(a) and II(a) for the 3-level DTC exhibit flux ripples of 0.0066Wb and 0.0047Wb, along with torque ripples of 0.183Nm and 0.154Nm, respectively, at the corresponding speeds. Likewise, I(b) and II(b) for the 5-level DTC showcase flux ripples of 0.005Wb and 0.00452Wb, as well as torque ripples of 0.112Nm and 0.106Nm, respectively, for speeds of 1400rpm and 100rpm. In contrast, the proposed DTC control scheme, represented by I(c) and II(c), achieves a notable reduction in flux ripple to 0.005Wb and 0.00354Wb, torque ripples of 0.042Nm and 0.046Nm, respectively, at the corresponding speeds of 1400rpm and 100rpm. This comparison highlights the superior performance of the proposed DTC method in minimizing both flux and torque ripples across different operational speeds under no load.

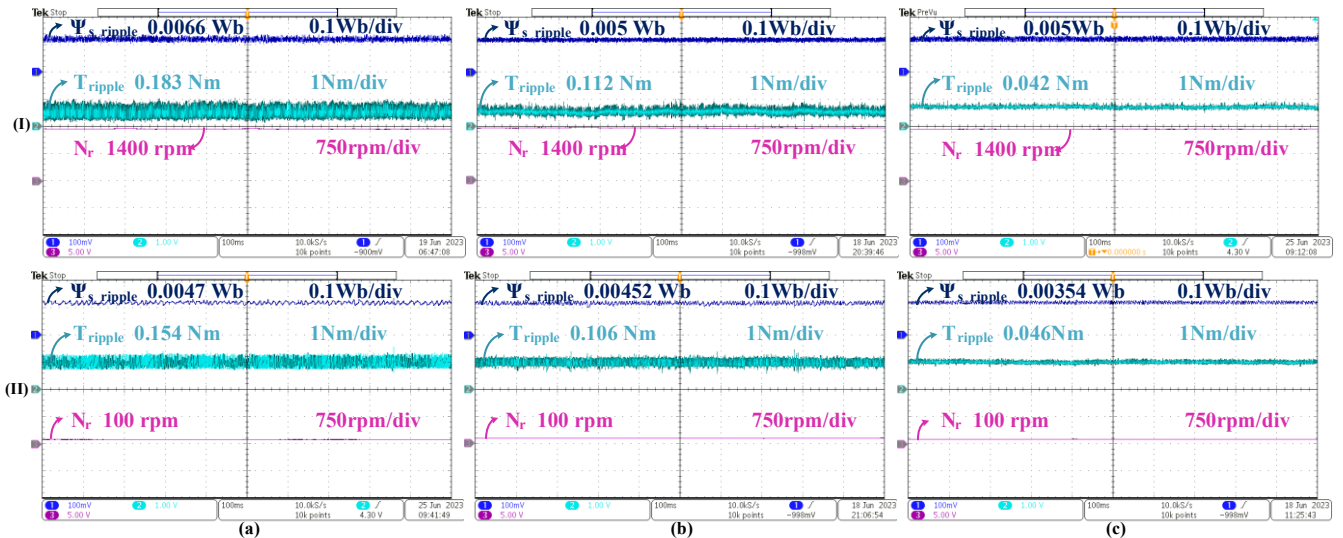


Fig. 8. Flux, torque pattern at no load for a speed of (I) 1400rpm, (II) 100rpm in (a) 3-level DTC [31], (b) 5-level DTC [33], (c) proposed DTC methods.

b) Loaded Condition: In response to an applied load of 2 Nm, Fig. 9 depicts the torque and flux patterns at speeds (I)

1400rpm and (II) 100rpm for (a) 3-level DTC [31], (b) 5-level DTC [33], and (c) the proposed DTC methods. In I(a) and

II(a), the 3-level DTC scheme demonstrates flux ripples of 0.0062Wb and 0.00445Wb, alongside torque ripples of 0.161Nm and 0.159Nm, respectively, corresponding to speeds of 1400rpm and 100rpm. Similarly, I(b) and II(b) for the 5-level DTC scheme show flux ripples of 0.0053Wb and 0.00443Wb, with torque ripples of 0.124Nm and 0.106Nm, respectively, at speeds of 1400rpm and 100rpm. Conversely, the proposed DTC scheme illustrated in I(c) and II(c) produces flux ripples of 0.0053Wb and 0.0037Wb, and torque ripples of 0.042Nm and 0.046Nm, respectively, at speeds of 1400rpm and 100rpm under the applied load of 2Nm. Fig. 9 vividly demonstrates that the proposed DTC control scheme exhibits notably reduced torque ripple at high

speeds and diminished torque and flux ripple at low speeds, under load conditions. In Fig. 10, the bar graph illustrates torque ripple at various speeds under a 2Nm load and no load for 3-level DTC [27], 5-level DTC [29], and the proposed DTC scheme. Notably, the suggested DTC control method markedly reduces torque ripple by employing a 7-level torque hysteresis controller at high speeds and a 3-level torque controller at low speeds with only small vectors. The proposed DTC contributes to the substantial improvement observed in minimizing torque ripple across a range of speeds and loading conditions, as highlighted in the graphical representation.

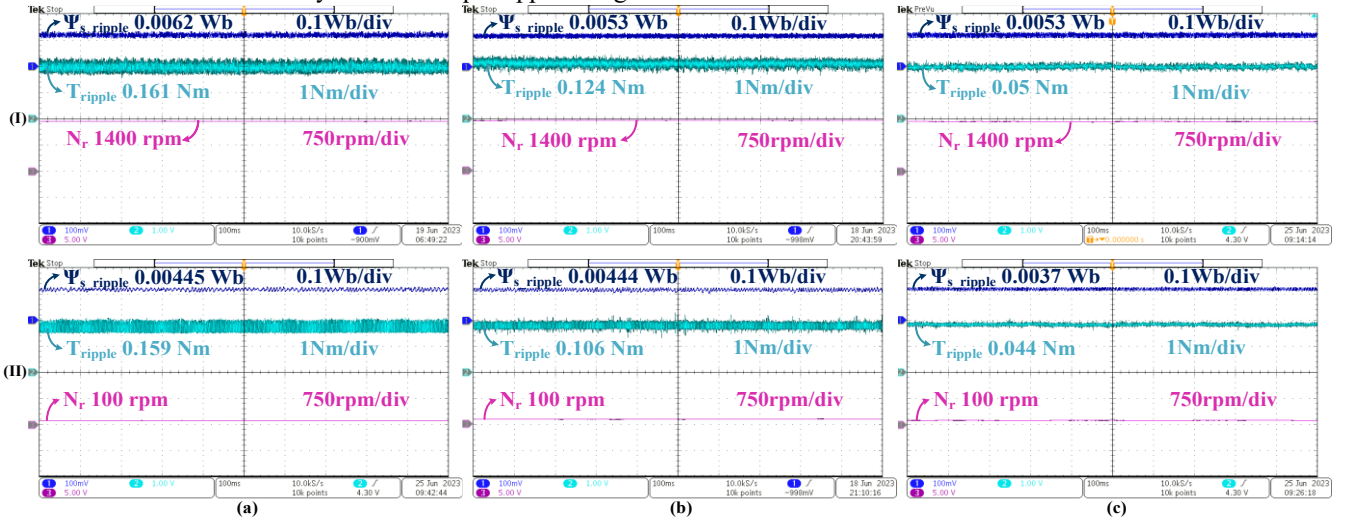


Fig. 9. Flux, torque pattern under the load of 2Nm for a speed of (I) 1400rpm, (II) 100rpm in (a) 3-level DTC [31], (b) 5-level DTC [33], (c) proposed DTC methods.

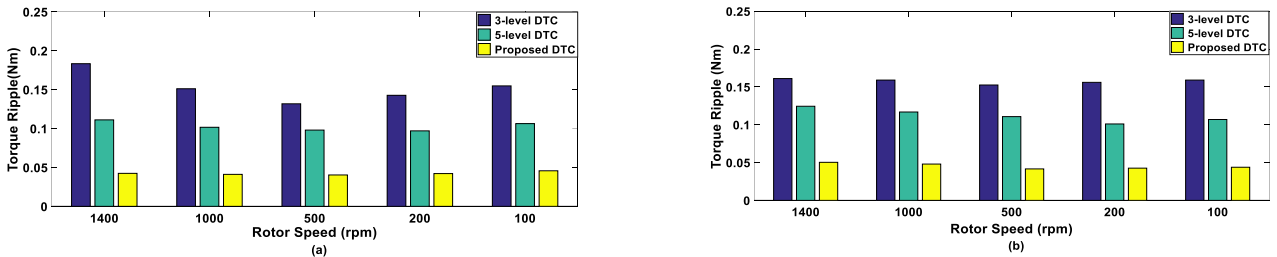


Fig. 10. Torque ripple analysis for different rotor speeds at (a) no load (b) load of 2 Nm for 3-level DTC[31], 5-level DTC[33], and proposed DTC scheme.

2) Current %THD Performance

Fig. 11 shows the fundamental currents ($\alpha\beta$ currents), and harmonic plane currents (xy) for the 3-level DTC, 5-level DTC, and proposed DTC scheme and it is observed that the proposed DTC scheme reduces harmonic plane currents w.r.t existing DTC methods. In Fig. 12, the phase current waveforms and their % Total Harmonic Distortion (%THD) are presented at speeds (I) 1400 rpm, and (II) 100 rpm for (a) 3-level DTC [31], (b) 5-level DTC [33], and (c) the proposed DTC method under a 2 Nm load. Examining I(a), and II(a), the 3-level DTC exhibits %THD values of 25.18%, and 27.93%, respectively, at speeds of 1400 rpm and 100 rpm. Similarly, in I(b), and II(bb), the 5-level DTC produces %THD values of 22.54%, and 19.35% for the corresponding speeds. In contrast, the proposed DTC scheme, as shown in I(c), and II(c) demonstrates %THD values of 18.04%, and 16.63%, respectively, for speeds of 1400 rpm, and 100 rpm under the 2 Nm load. Fig. 13 further presents a bar graph depicting the phase current harmonic

distortion at various rotor speeds under an applied load of 2 Nm. It is evident from the graph that the proposed DTC control method consistently exhibits reduced harmonic current distortion when compared with the 3-level DTC [31] and 5-level DTC [33] methods. This signifies a notable improvement in the current quality achieved by the proposed control approach. From the analysis of Fig. 8- Fig. 13, and the results comparison Table III, it is evident that the proposed Direct Torque Control (DTC) scheme for a dual 2-level inverter-controlled 5-phase induction motor (DI-FPOEWIM) outperforms the existing DTC techniques [31], [33]. The introduction of a 7-level torque controller in the proposed DTC scheme leads to a significant reduction in the current % Total Harmonic Distortion (%THD) and torque ripple. Furthermore, the utilization of a 3-level torque controller with small vectors and null vectors in the proposed scheme contributes to a simultaneous reduction in both torque and flux ripple, along with a notable decrease in current harmonic distortion compared to existing methods.

These findings underscore the superior performance and efficiency of the proposed DTC approach in optimizing the steady-state operation of the DI-FPOEWIM. The parameters for the 5-phase open-end winding induction motor and the control algorithm parameters are outlined in Table IV.

B. Dynamic Response Analysis

The dynamic performance of the proposed DTC control scheme is tested and compared with the classical DTC

schemes in [31], [33] to know dynamic behavior of proposed method for speed and load disturbances. The implementation of the DTC control algorithm in the 3-level DTC [31], 5-level DTC [33], and proposed DTC scheme implemented by the same hysteresis band, DC voltage source, and sampling time. This uniformity makes, these three methods showcasing identical dynamics in the induction motor as discussed below.

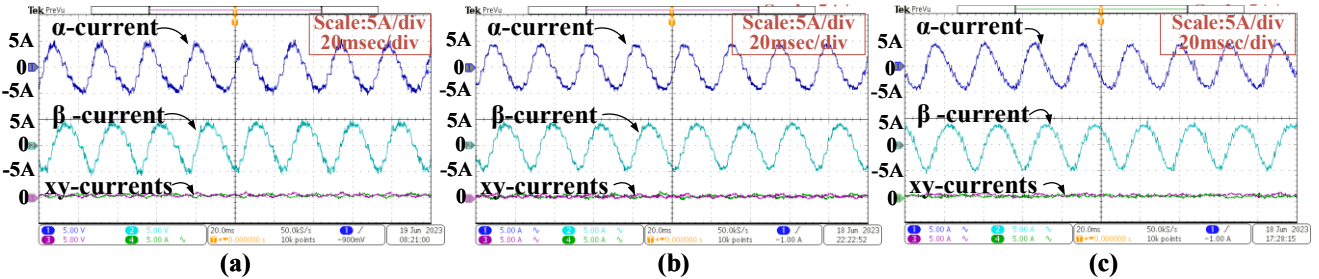


Fig. 11. Fundamental plane (α,β) currents and harmonic plane (x,y) currents for (a) 3-level DTC[31], (b) 5-level DTC[33] (c) proposed DTC scheme.

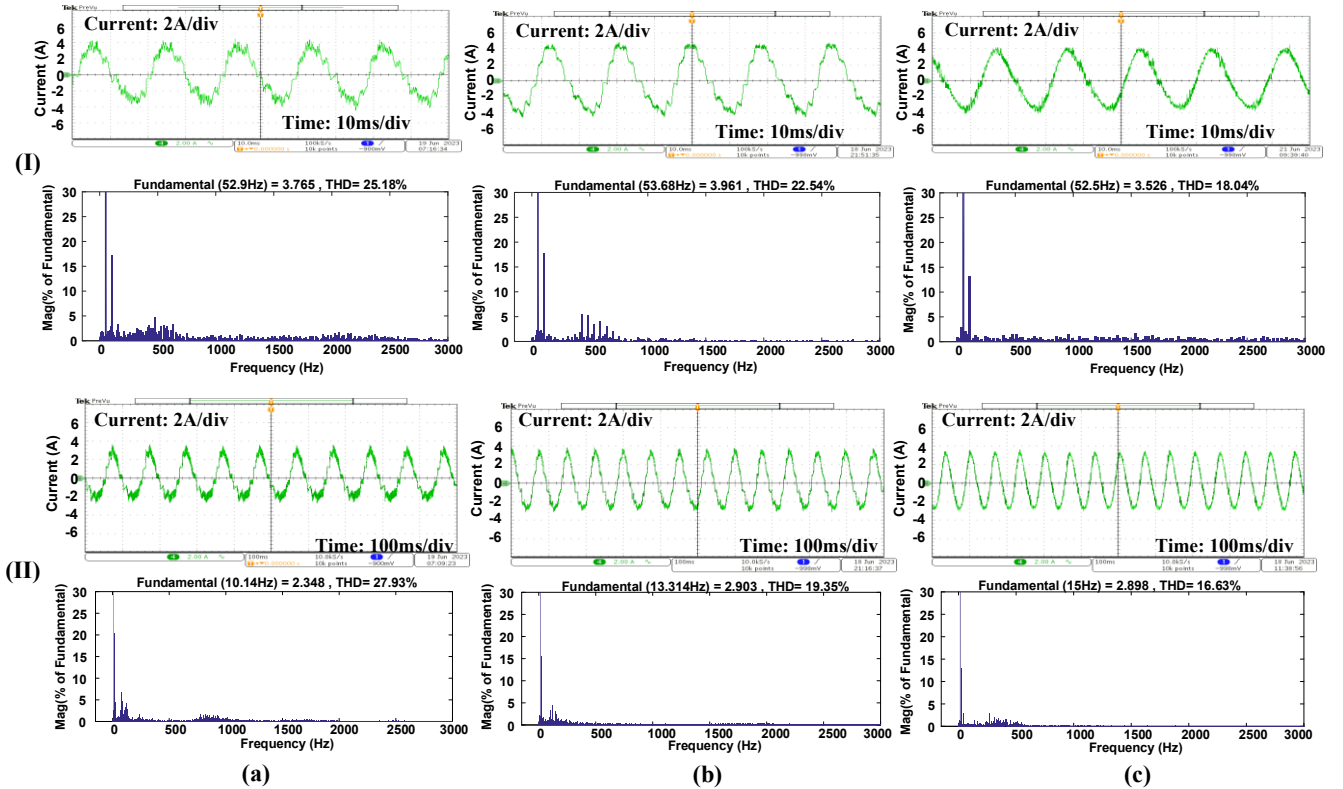


Fig. 12. Current waveform and %THD for a speed of (I) 1400rpm, (II) 100rpm at load 2Nm for (a) 3-level DTC[31], (b) 5-level DTC[33], (c) proposed DTC schemes.

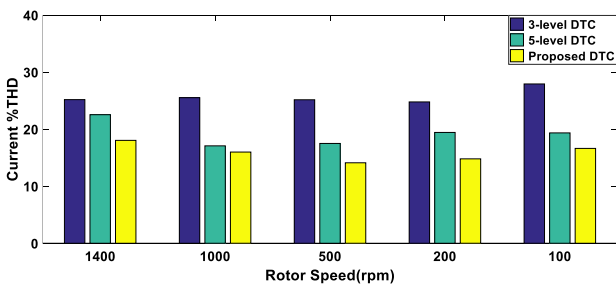


Fig. 13. Current %THD analysis for various speeds under 2Nm load for 3-level DTC, 5-level DTC, proposed DTC scheme.

1) Speed Dynamics

In Fig. 14, it displays the speed reversal disturbance from -500 rpm to 500 rpm for three control methods on a DI-FPOEWIM: (a) 3-level DTC, (b) 5-level DTC, and (c) the proposed DTC scheme. It's noticeable that the proposed method exhibits a speed reversal response similar to existing DTC control techniques. Likewise, Fig. 15 illustrates speed disturbances from 1000 rpm to 1400 rpm for (a) 3-level DTC, (b) 5-level DTC, and (c) the proposed DTC method and it is seen that the proposed DTC scheme shows a response similar to other existing DTC methods [31] and [33].

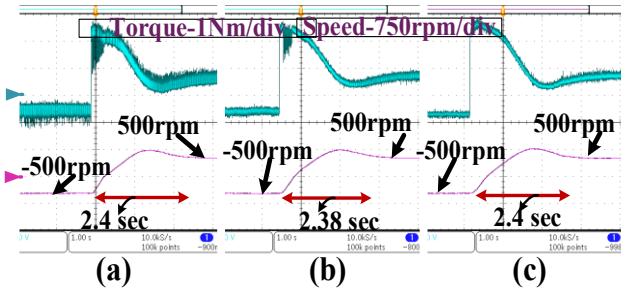


Fig. 14. Step speed reversal response from -500 rpm to 500 rpm at no load (a)3-level DTC (b) 5-level DTC (c) proposed DTC schemes.

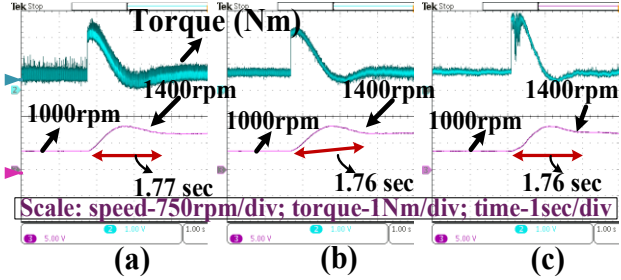


Fig. 15. Speed response from 1000 rpm to 1400 rpm at no load (a)3-level DTC (b) 5-level DTC (c) proposed DTC schemes.

From Fig. 14 and Fig. 15, it is concluded that the proposed DTC scheme does not negatively affect the fast-speed dynamics.

2) Load Torque Dynamics

The inspection of torque dynamics involves introducing load disturbances, from no load to a 2 Nm load, for different control methods of the dual inverter-fed 5-phase induction motor, as depicted in Fig. 16: (a) 3-level DTC, (b) 5-level DTC, and (c) the proposed DTC scheme. It's evident from Fig. 16 that the proposed DTC scheme exhibits a response similar to existing DTC schemes mentioned in references [31] and [33].

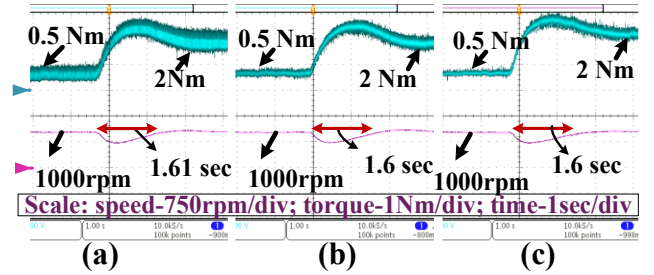


Fig. 16. Step load disturbance response from no load to 2 Nm at 1000 rpm (a)3-level DTC[31] (b) 5-level DTC[33] (c) proposed DTC schemes.

TABLE III
TORQUE RIPPLE AND %THD COMPARISON TABLE FOR 3-LEVEL DTC, 5-LEVEL DTC, AND PROPOSED DTC SCHEMES FOR VARIOUS SPEEDS

Scheme	1400 rpm		1000 rpm		500 rpm		100 rpm	
	T_{ripple} (Nm)	THD (%)	T_{ripple} (Nm)	THD (%)	T_{ripple} (Nm)	THD (%)	T_{ripple} (Nm)	THD (%)
3-level DTC scheme [33]	0.161	25.18	0.159	25.52	0.1525	25.16	0.159	27.93
5-level DTC scheme [31]	0.1244	22.54	0.1168	19.85	0.1107	17.50	0.1069	19.35
Proposed DTC scheme	0.0503	18.04	0.048	15.99	0.0416	14.11	0.0438	16.63
% ripple, %THD reduction w.r.t 3-level DTC scheme	68.7%	28.3%	68.5%	37.3%	72.7%	43.9%	72.3%	40.4%
% ripple, %THD reduction w.r.t 5-level DTC scheme	59.5%	19.9%	58.9%	19.44%	62.4%	19.3%	58.8%	14.0%

TABLE IV
FIVE-PHASE OPEN-END WINDING INDUCTION MOTOR (FPOEWIM) PARAMETERS

Parameter	value	Parameter	Value	Parameter	Value
Power Rating	1 HP	Stator resistance (R_s)	1.05 Ω	Rotor resistance (R_r)	1.42 Ω
Stator inductance (L_s)	90.73mH	Mutual inductance (L_m)	84.73mH	Rotor inductance (L_r)	90.73mH
No. of Poles (P)	4	Inertia constant (J)	0.148Kg-m ²	Rated Speed	1400 rpm
DC voltage (V_{dc})	110V	Sample time (T_s)	100e-6 sec	PI controller K_p, K_i	0.02, 0.005

V. CONCLUSIONS

The proposed Direct Torque Control (DTC) technique for a dual 5-leg inverter FPOEWIM introduces a novel approach by employing a 7-level torque hysteresis controller at high speeds and a 3-level torque hysteresis controller at low speeds, supplemented by the same 2-level flux hysteresis controller to mitigate flux and torque ripple and reduce current harmonic distortion. The use of 30 virtual voltage vectors optimizes the torque controllers while enhancing DC bus utilization compared to single inverter-controlled induction motors. Thoroughly tested across various speeds and loads, the scheme demonstrates improved steady-state performance, notably reduced current harmonic distortion and torque ripple under high-speed conditions, with and without a load, facilitated by a modified 7-level hysteresis controller. A modified lookup table, featuring a 3-level torque controller under low speeds, minimizes both torque and flux ripple under

different loading conditions. The proposed control scheme produces zero common mode voltage which enables the utilization of a single common DC bus without requiring an isolation transformer, while concurrently eliminating harmonic plane (xy-plane) components through a volt-sec balance scheme. The proposed control method of a 5-phase induction motor is particularly well-suited for applications in high torque density industrial drives, electric aircraft, and electric vehicles, showcasing superior reliability, increased torque density, efficient space utilization, lower voltage rating, and minimized torque and flux ripples.

REFERENCES

- [1] 'Multiphase induction motor drives – a technology status review' E. Levi, R. Bojoi, F. Profumo, H.A. Toliyat and S. Williamson IET Electr. Power Appl., 2007, 1, (4), pp. 489–516
- [2] E. Levi, "Multiphase Electric Machines for Variable-Speed Applications," in IEEE Transactions on Industrial Electronics,

- vol. 55, no. 5, pp. 1893-1909, May 2008, doi: 10.1109/TIE.2008.918488.
- [3] M. Mengoni, L. Zarri, A. Tani, L. Parsa, G. Serra, and D. Casadei, "High-Torque-Density Control of Multiphase Induction Motor Drives Operating Over a Wide Speed Range," in *IEEE Transactions on Industrial Electronics*, vol. 62, no. 2, pp. 814-825, Feb. 2015, doi: 10.1109/TIE.2014.2334662.
 - [4] N. Bianchi, S. Bolognani and M. Dai Pre, "Strategies for the Fault-Tolerant Current Control of a Five-Phase Permanent-Magnet Motor," in *IEEE Transactions on Industry Applications*, vol. 43, no. 4, pp. 960-970, July-Aug. 2007, doi: 10.1109/TIA.2007.900445.
 - [5] A. Tani, M. Mengoni, L. Zarri, G. Serra and D. Casadei, "Control of Multiphase Induction Motors With an Odd Number of Phases Under Open-Circuit Phase Faults," in *IEEE Transactions on Power Electronics*, vol. 27, no. 2, pp. 565-577, Feb. 2012, doi: 10.1109/TPEL.2011.2140334.
 - [6] S. Williamson and S. Smith, "Pulsating torque and losses in multiphase induction machines," *Conference Record of the 2001 IEEE Industry Applications Conference. 36th IAS Annual Meeting (Cat. No.01CH37248)*, Chicago, IL, USA, 2001, pp. 1155-1162 vol.2, doi: 10.1109/IAS.2001.955635.
 - [7] A. Baltatanu and M. -L. Florea, "Multiphase machines used in electric vehicles propulsion," *Proceedings of the International Conference on ELECTRONICS, COMPUTERS, and ARTIFICIAL INTELLIGENCE - ECAI-2013*, 2013, pp. 1-6, doi: 10.1109/ECAI.2013.6636204.
 - [8] Wang, Fengxiang & Zhang, Zhenbin & Mei, Xuezhu & Rodriguez, Jose & Kennel, Ralph. (2018). *Advanced Control Strategies of Induction Machine: Field Oriented Control, Direct Torque Control, and Model Predictive Control*. Energies. 11. 10.3390/en11010120.
 - [9] S. Devabhaktuni and R. G., "Performance analysis of three-phase and five-phase inverters with different PWM strategies," *2019 Innovations in Power and Advanced Computing Technologies (i-PACT)*, 2019, pp. 1-5, doi: 10.1109/i-PACT44901.2019.8960210.
 - [10] A. Bhowate, M. V. Aware, and S. Sharma, "Predictive Torque Control Algorithm for a Five-Phase Induction Motor Drive for Reduced Torque Ripple With Switching Frequency Control," in *IEEE Transactions on Power Electronics*, vol. 35, no. 7, pp. 7282-7294, July 2020, doi: 10.1109/TPEL.2019.2954991.
 - [11] I. Takahashi and T. Noguchi, "A New Quick-Response and High-Efficiency Control Strategy of an Induction Motor," in *IEEE Transactions on Industry Applications*, vol. IA-22, no. 5, pp. 820-827, Sept. 1986, doi: 10.1109/TIA.1986.4504799.
 - [12] M. Bertoluzzo, G. Buja and R. Menis, "Analytical formulation of the direct control of induction motor drives," *ISIE '99. Proceedings of the IEEE International Symposium on Industrial Electronics (Cat. No.99TH8465)*, 1999, pp. PS14-PS20 vol.1, doi: 10.1109/ISIE.1999.801745.
 - [13] V. Ambrozic, G. S. Buja and R. Menis, "Band-constrained technique for direct torque control of induction motor," in *IEEE Transactions on Industrial Electronics*, vol. 51, no. 4, pp. 776-784, Aug. 2004, doi: 10.1109/TIE.2004.831722.
 - [14] L. Parsa and H. A. Toliyat, "Sensorless Direct Torque Control of Five-Phase Interior Permanent-Magnet Motor Drives," in *IEEE Transactions on Industry Applications*, vol. 43, no. 4, pp. 952-959, July-Aug. 2007, doi: 10.1109/TIA.2007.900444.
 - [15] L. Zheng, J. E. Fletcher, B. W. Williams, and X. He, "A Novel Direct Torque Control Scheme for a Sensorless Five-Phase Induction Motor Drive," in *IEEE Transactions on Industrial Electronics*, vol. 58, no. 2, pp. 503-513, Feb. 2011, doi: 10.1109/TIE.2010.2047830.
 - [16] L. Gao, J. E. Fletcher, and L. Zheng, "Low-Speed Control Improvements for a Two-Level Five-Phase Inverter-Fed Induction Machine Using Classic Direct Torque Control," in *IEEE Transactions on Industrial Electronics*, vol. 58, no. 7, pp. 2744-2754, July 2011, doi: 10.1109/TIE.2010.2070775.
 - [17] S. Payami and R. K. Behera, "An Improved DTC Technique for Low-Speed Operation of a Five-Phase Induction Motor," in *IEEE Transactions on Industrial Electronics*, vol. 64, no. 5, pp. 3513-3523, May 2017, doi: 10.1109/TIE.2017.2652397.
 - [18] V. S. Reddy and S. Devabhaktuni, "Enhanced Low-Speed characteristics with Constant Switching Torque Controller-based DTC Technique of Five-Phase Induction Motor Drive with FOPI Control," in *IEEE Transactions on Industrial Electronics*, doi: 10.1109/TIE.2022.3227275.
 - [19] Yen-Shin Lai and Jian-Ho Chen, "A new approach to direct torque control of induction motor drives for constant inverter switching frequency and torque ripple reduction," in *IEEE Transactions on Energy Conversion*, vol. 16, no. 3, pp. 220-227, Sept. 2001, doi: 10.1109/60.937200.
 - [20] Atif Iqbal & Emil Levi (2006) *Space Vector PWM Techniques for Sinusoidal Output Voltage Generation with a Five-Phase Voltage Source Inverter*, *Electric Power Components, and Systems*, 34:2, 119-140, DOI: 10.1080/15325000500244427
 - [21] Venkata Subba Reddy C, Swati Devabhaktuni. "Low-speed Performance improvement of Constant Switching Frequency DTC of Five-Phase Induction Motor", *2021 National Power Electronics Conference (NPEC)*, 2021
 - [22] H. Ismail et al., "Direct Torque Control of induction machine using 3-level neutral point clamped inverter," *2015 IEEE Student Conference on Research and Development (SCORED)*, Kuala Lumpur, Malaysia, 2015, pp. 571-576, doi: 10.1109/SCORED.2015.7449401.
 - [23] F. Khoucha, S. M. Lagoun, K. Marouani, A. Kheloui and M. E. H. Benbouzid, "Hybrid Cascaded H-Bridge Multilevel-Inverter Induction-Motor-Drive Direct Torque Control for Automotive Applications," in *IEEE Transactions on Industrial Electronics*, vol. 57, no. 3, pp. 892-899, March 2010, doi: 10.1109/TIE.2009.2037105.
 - [24] M. F. Escalante, J. . -C. Vannier and A. Arzande, "Flying capacitor multilevel inverters and DTC motor drive applications," in *IEEE Transactions on Industrial Electronics*, vol. 49, no. 4, pp. 809-815, Aug. 2002, doi: 10.1109/TIE.2002.801231.
 - [25] Y. N. Tatte and M. V. Aware, "Torque Ripple and Harmonic Current Reduction in a Three-Level Inverter-Fed Direct-Torque-Controlled Five-Phase Induction Motor," in *IEEE Transactions on Industrial Electronics*, vol. 64, no. 7, pp. 5265-5275, July 2017, doi: 10.1109/TIE.2017.2677346.
 - [26] S. Payami, R. K. Behera and A. Iqbal, "DTC of Three-Level NPC Inverter Fed Five-Phase Induction Motor Drive With Novel Neutral Point Voltage Balancing Scheme," in *IEEE Transactions on Power Electronics*, vol. 33, no. 2, pp. 1487-1500, Feb. 2018, doi: 10.1109/TPEL.2017.2675621.
 - [27] R. E. Kodumur Meesala and V. K. Thippiripati, "An Improved Direct Torque Control of Three-Level Dual Inverter Fed Open-Ended Winding Induction Motor Drive Based on Modified Look-Up Table," in *IEEE Transactions on Power Electronics*, vol. 35, no. 4, pp. 3906-3917, April 2020, doi: 10.1109/TPEL.2019.2937684.
 - [28] R. Karampuri, S. Jain and V. T. Somasekhara, "Common-Mode Current Elimination PWM Strategy Along With Current Ripple Reduction for Open-Winding Five-Phase Induction Motor Drive," in *IEEE Transactions on Power Electronics*, vol. 34, no. 7, pp. 6659-6668, July 2019, doi: 10.1109/TPEL.2018.2873692.
 - [29] R. Karampuri, S. Jain and V. T. Somasekhara, "Sample-Averaged Zero-Sequence Current Elimination PWM Technique for Five-Phase Induction Motor With Opened Stator Windings," in *IEEE Journal of Emerging and Selected Topics in Power Electronics*, vol. 6, no. 2, pp. 864-873, June 2018, doi: 10.1109/JESTPE.2017.2759965.
 - [30] Reddy, C.V.S., Devabhaktuni, S. (2022). *Low-Speed Performance Improvement of Dual VSI Fed Direct Torque Controlled Five Phase Open-End Winding Induction Motor*. In: Kumar, S., Singh, B., Singh, A.K. (eds) *Recent Advances in Power Electronics and Drives. Lecture Notes in Electrical Engineering*, vol 852. Springer, Singapore. https://doi.org/10.1007/978-981-16-9239-0_20.
 - [31] P. C. Mavila and P. P. Rajeevan, "A New Direct Torque Control Scheme for Five Phase Open-end Winding Induction Motor Drives with Reduced DC Voltage Requirement," *2020 IEEE International Conference on Power Electronics, Smart Grid and Renewable Energy (PESGRE2020)*, Cochin, India, 2020, pp. 1-6, doi: 10.1109/PESGRE45664.2020.9070665.

- [32] P. C. Mavila and P. P. Rajeevan, "A Five Level DTC Scheme for Dual Inverter-Fed Five Phase Open-End Winding Induction Motor Drives with Single DC Source," 2019 IEEE Industry Applications Society Annual Meeting, Baltimore, MD, USA, 2019, pp. 1-6, doi: 10.1109/IAS.2019.8912445
- [33] P. C. Mavila and P. P. Rajeevan, "A Five-Level Torque Controller Based DTC Scheme for Open-End Winding Five-Phase IM Drive With Single DC Source and Auxiliary Plane Harmonic Elimination," in IEEE Transactions on Industry Applications, vol. 58, no. 2, pp. 2063-2074, March-April 2022, doi: 10.1109/TIA.2022.3140361.
- [34] V. S. Reddy C and S. Devabhaktuni, "Improved Low-Speed Performance of DTC controller-based Dual Voltage Source Inverter fed Five-Phase OEW Induction Motor," 2022 IEEE International Conference on Power Electronics, Drives and Energy Systems (PEDES), Jaipur, India, 2022, pp. 1-4, doi: 10.1109/PEDES56012.2022.10080521.



Venkata Subba Reddy C. was born in Kadapa, India in 1991. He received his Master's Degree (2015) in Power Electronics Drives from RGM CET Nandyal. Currently, he is working towards a Ph.D. degree from the Electrical Engineering Department, National Institute of Technology,

Warangal, India. His current research work interests are speed control of multi-phase drives.



Swati Devabhaktuni received a Ph.D. degree in electrical engineering from the JNT University, Hyderabad in 2014. Currently, she is working as an Assistant professor at the National Institute of Technology, Warangal. Her research interests are power electronics, AC motor drives, and control system.